The Application of X-ray, NMR, and Molecular Modeling in the Design of MMP Inhibitors

Thomas S. Rush III[1,*] and Robert Powers[1,2]

[1]*Structural Biology & Computational Chemistry, Department of Chemical & Screening Sciences, Wyeth Research, 87 Cambridge Park Dr. Cambridge, MA, 02140, USA and* [2]*Current address: University of Nebraska-Lincoln, Department of Chemistry, Lincoln, NE 68588, USA*

Abstract: The following review discusses the successful application of X-ray, NMR, and molecular modeling in the design of potent and selective inhibitors of matrix metalloproteinases (MMPs) and TNFα-converting enzyme (TACE) from Wyeth. The importance of protein and ligand mobility as it impacts structure-based design is also discussed. The MMPs are an active target for a variety of diseases, including cancer and arthritis.

Key Words: Structure-based drug design, Matrix Metalloproteinase, Matrix Metalloprotease, X-ray, NMR, Molecular Modeling, Inhibitor, MMP

INTRODUCTION

The matrix metalloproteinases (MMPs) are a family of zinc-containing proteins that are involved in the degradation of extracellular matrices, and are consequently associated with normal tissue remodeling processes such as pregnancy, wound healing, apoptosis, and angiogenesis [1-3]. The MMPs have also demonstrated activity against cell surface and other pericellular non-matrix proteins, further contributing to their battery of functions [4]. Overall, the MMP family consists of more than 25 enzymes, with differences in substrate preference (collagens, fibronectin, elastin, gelatins, etc.), domain structure and sequence homology [5]. As depicted in Figs. (**1**) and (**2**), the MMPs are multidomain proteins, with a signal peptide, propeptide and catalytic domain that are common to the entire family [6]. Additional domains observed in MMP structures include fibronectin type II-like, hemopexin-like, vitronectin-like and transmembrane domains.

Fundamental to the structural integrity and catalytic activity of MMPs is the presence of both zinc and calcium in the protein's structure. The active site zinc performs a critical function for both substrate binding and cleavage (see Fig. (**3**)). Correspondingly, the design of MMP inhibitors has generally targeted the catalytic domain and active site zinc [5,7]. In some cases, the isolated catalytic domain maintains its general endopeptidase function but does not exhibit activity against its natural substrate. This is attributed to the absence of other domains, which are presumably involved in substrate recognition and binding.

As a result of the degradative nature of MMP enzymes, their expression and activity is tightly controlled through a number of internal mechanisms. The MMPs are regulated by either naturally expressed small-protein inhibitors, called tissue inhibitor of metalloproteinases (TIMPs), the presence or absence of the propeptide domain, or by natural transcription induction/suppression mechanisms [8]. The latter include normal stimuli such as cytokines and hormones, but may also include oncogene products and tumor promoters [9,10]. Uncontrolled, aberrant matrix degradation by the MMPs has been implicated in a variety of diseases with cancer and arthritis receiving the most attention [11,12]. The MMPs have also been associated with multiple sclerosis [13], periodontitis [14], stroke [15], inflammatory bowel disease [16] and cardiovascular disease [17]. The broad association between MMP catalytic activity and a number of serious diseases has made the MMPs an attractive target for structure-based drug design [5,7].

Toward this end, there have been numerous structures determined for the catalytic domain of various MMPs complexed with a variety of natural and synthetic inhibitors [5]. [Since the writing of reference 5, new MMP catalytic domain structures in the Protein Data Bank include: 1GKC, and 1L6J (MMP9), 1HV5 (MMP-11), 1JIZ, 1JK3 (MMP-12)] In general, the various MMP catalytic domain structures reveal a close similarity in their overall three-dimensional fold (Fig. (**4**)), consistent with the relatively high sequence homology across the family (Fig. (**2**)).

Despite their structural similarity, subgroups and even individual MMPs have distinct substrate specificity, which is associated with their unique biological functions and corresponding roles in related disease processes. Examples of this disease specificity include the over-expression of MMP-13 in breast carcinoma and MMP-1 in papillary carcinomas. Further supporting the unique roles for the various MMPs is the variety of transgenic mice that are either MMP deficient, TIMP deficient, MMP over-expressing or TIMP over-expressing that exhibit distinct phenotypes associated with each MMP or TIMP protein [3,5]. Therefore, to minimize potential side effects, one paradigm in the development of MMP inhibitors as therapeutic agents is to design specificity

*Address correspondence to this author at Structural Biology & Computational Chemistry, Department of Chemical & Screening Sciences, Wyeth Research, 87 Cambridge Park Dr. Cambridge, MA, 02140, USA; E-mail: trush@wyeth.com

1568-0266/04 $45.00+.00

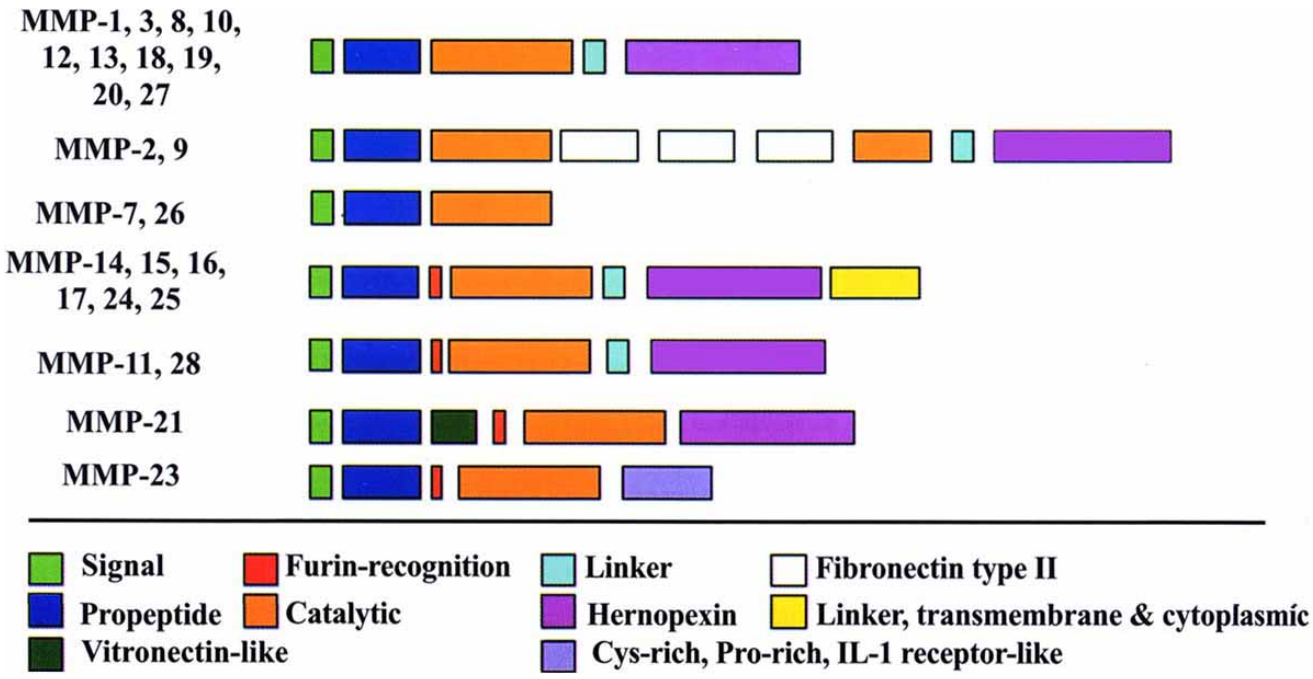

Fig. (1). The domain structures of the MMPs.

into the structures of the small molecule instead of developing a broad-spectrum inhibitor [18,19]. To do so, it is extremely beneficial to obtain extensive static and dynamic structural information for the various MMPs in a variety of states [18-22].

Fortunately for researchers currently designing MMP inhibitors, there is a generous amount of structural data readily available for a number of the MMPs. These structures have clearly identified both common features and significant differences in the active sites, which may be exploited in the structure-based design process. In general, the active site zinc of an MMP is coordinated to three histidine side chains. In the enzyme's resting state, the zinc also coordinates a water molecule that is to be used to hydrolyze the substrate's peptide bond. The water molecule is also held in place by the side chain of an active site glutamic acid (Fig. (**3**)). Another basic feature of the MMP active site is the presence of three substrate-binding subsites to the left (unprimed side) and right (primed side) of the catalytic zinc. These subsites accommodate the side chains of the peptide to be cleaved, and the local structural characteristics and electrostatic environment of the individual subsites effectively determine substrate specificity. In particular, comparison of the various MMP structures has identified significant differences in the sizes and shapes of the S1' pocket of a number of the MMPs (Fig. (**5**)) [5,7].

This major structural difference provides an obvious approach for designing specificity into potent MMP inhibitors, which is to develop compounds that appropriately fill the available space in the S1' pocket while taking advantage of unique chemical environments afforded by specific amino acid differences [20,21,23]. This review describes Wyeth's early efforts in using experimental structural information and molecular modeling to design high-affinity and specific MMP inhibitors for the treatment of arthritis (Fig. (**6**)).

3D STRUCTURE OF THE MMP CATALYTIC DOMAINS

It is well established that type II collagen is an important molecule in articular cartilage, and that the joint damage associated with osteoarthritis is correlated with its degradation. It has been found that this process correlates with increased production of various MMPs [24], specifically the collagenases (MMP-1, MMP-8 and MMP-13). For the treatment of osteoarthritis (OA), most recent drug development efforts have focused on designing inhibitors of the catalytic domain of MMP-13, due to its high level of activity and specificity against type II collagen. In addition, it has been observed that IL-1 and TNF, which induce MMP-13 production and activation in osteoblasts and chondrocytes, are elevated during disease [25,26].

Recent clinical trials evaluating the utility of MMP inhibitors in both cancer and arthritis treatment have been plagued by the occurrence of musculoskeletal side effects [27,28]. It has been proposed by some that these dose-related symptoms are related to the non-specific binding and inhibition of other MMPs. In particular, it has been suggested that some of the side effects seen in clinical trials of MMP inhibitors may be specifically related to MMP-1, MMP-14 [29-31] or sheddase inhibition [32]. Thus, our approach to the development of an osteoarthritis treatment relied on the structure-based design of inhibitors of MMP-13 with selectivity over MMP-1 as a minimum requirement, and selectivity over all other zinc endopeptidases as a desirable goal [33]. Consequently, we examined the structure of a number of MMPs (MMP-1, MMP-9, MMP-12, MMP-13), with and without bound inhibitors.

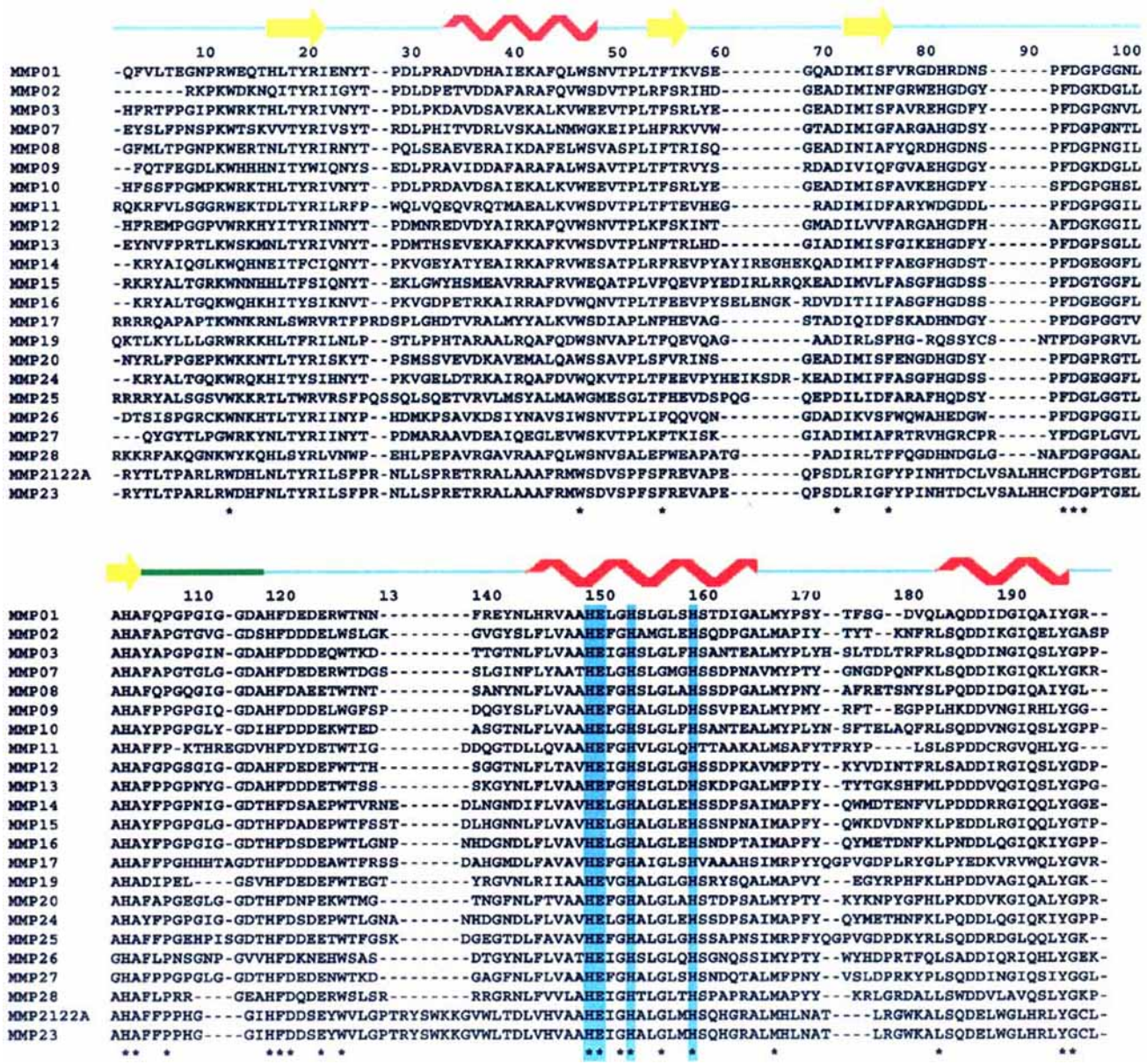

Fig. (2). A Structural alignment of catalytic domains of the MMPs, guided by publicly available MMP structures. The residue numbering refers to the numbering in our MMP-1 NMR structure. Conserved residues are indicated with an asterisk at the bottom of the alignment, and the active site histidines and glutamic acid are highlighted in blue.

Initially, three structurally diverse inhibitors were available for use in the study of these enzymes and the subsequent design of inhibitors of MMP-13 and TACE, a related protein. Sulfonamide hydroxamate **1** (Fig. **6**), CGS 27023A, was the first reported non-peptide MMP inhibitor, and has been in clinical trials for the treatment of cancer. It is a potent, broad spectrum MMP inhibitor. The anthranilate-based sulfonamide hydroxamate, **2**, has a longer and more rigid linker between the zinc chelator and the sulfonamide oxygens than CGS 27023A. Compound **2** is also a broad spectrum MMP inhibitor, with low nanomolar IC_{50}s against MMP-1, -9 and -13. The third variation is the sulfone hydroxamate, **3**, with only one atom separating the hydroxamate and the requisite sulfone hydrogen bond acceptor.

Our structure-based design effort began with the high-resolution solution NMR structure of inhibitor-free MMP-1 [34,35]. This represented the first structure of an uncomplexed MMP, providing a unique insight into the architecture and behavior of the active site in the absence of an inhibitor. Additionally, it provided a ready mechanism to rapidly determine further structures of MMP-1/inhibitor complexes and to analyze differences between the bound and free forms of the protein [36]. Furthermore, the availability of the MMP-1 NMR structure provided an effective means to design selective MMP-13 inhibitors by comparing the features of both the MMP-1 and MMP-13 structures, and the behavior of inhibitors bound to the two proteins.

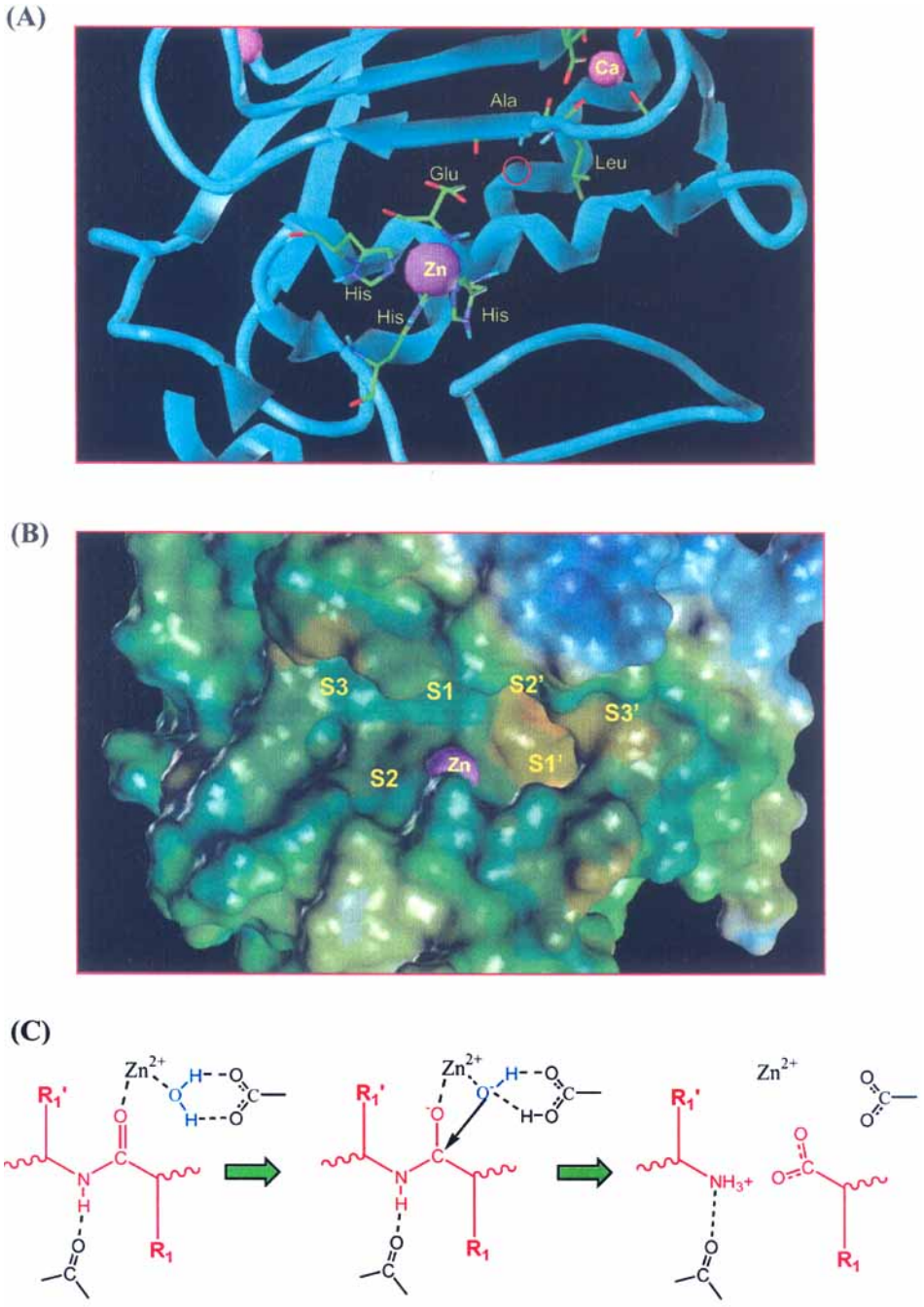

Fig. (3). A general representation of the structure and catalytic mechanism of the MMPs. (A) A ribbon representation of the active site highlighting important residues and the hydrogen bond acceptor "hot spot" discussed in the text. (B) A surface representation of the active site, highlighting the catalytic zinc and its relationship to the substrate sidechain binding pockets. The protein is represented by its solvent accessible surface, which is colored by lipophilic potential [brown = hydrophobic, blue = hydrophilic]. (C) A general outline of the catalytic mechanism of the MMPs.

Overall, the structure of the catalytic domain of MMP-1 is typical of the MMPs (Fig. (**4**)). The general tertiary structure consists of a five stranded mixed parallel and anti-parallel β-sheet, comprised of 4-7 residues per β-strand, and three α-helices comprised of 11-17 residues per helix. The active site of MMP-1 is bordered by β-strand IV, the Ca^{+2} binding loop, helix B, and a random coil region. The catalytic zinc is chelated by H118, H122, and H128, while H68, H83 and H96 chelate the structural zinc. The calcium ion is chelated in a loop region consisting of residues D75 to G79. An interesting feature of the MMP-1 active site is an apparent kink in the backbone that occurs at L81 between the Ca^{+2} binding loop and β-strand IV. This results in the NH of both L81 and A82 facing toward the active site of the enzyme, providing an active site acceptor "hot spot". Additionally, the calcium ion is likely pulling electrons out

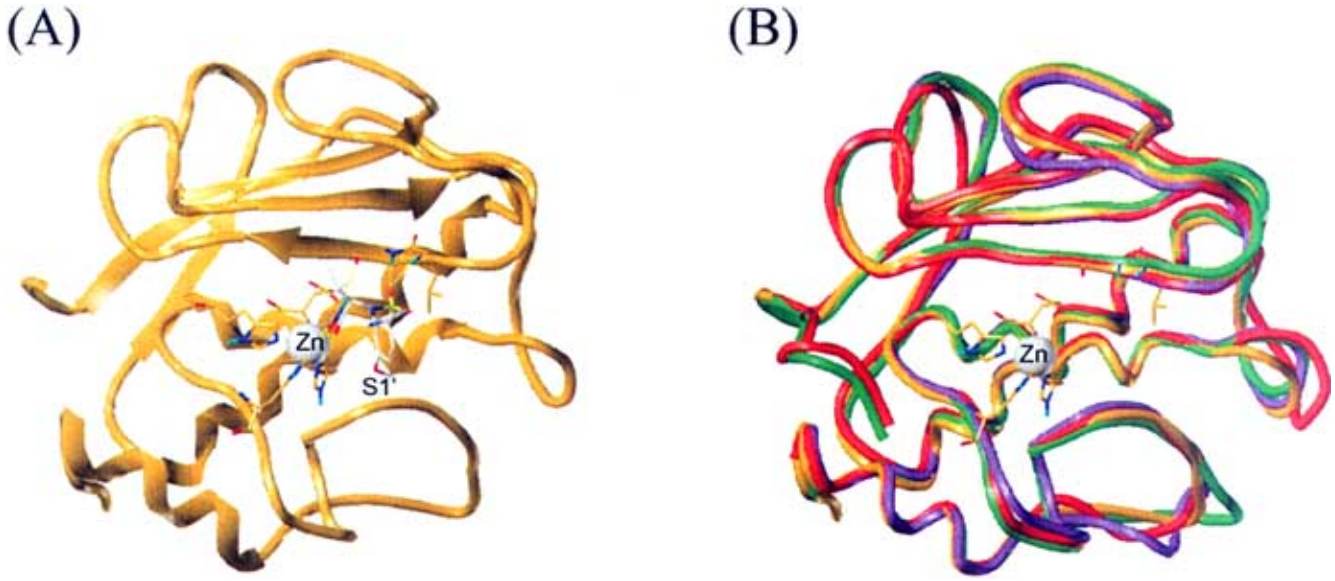

Fig. (4). (a) Ribbon drawing of the NMR structure of the MMP-1:CGS-27023A (2); the protein is depicted in orange, and the inhibitor in white. Yellow dotted lines indicated electrostatic and hydrogen bond interactions with the protein as discussed in text. (b) overlay of the backbone atoms for MMP-1 (orange), MMP-9 (red), MMP-12 (purple) and MMP-13 (green).

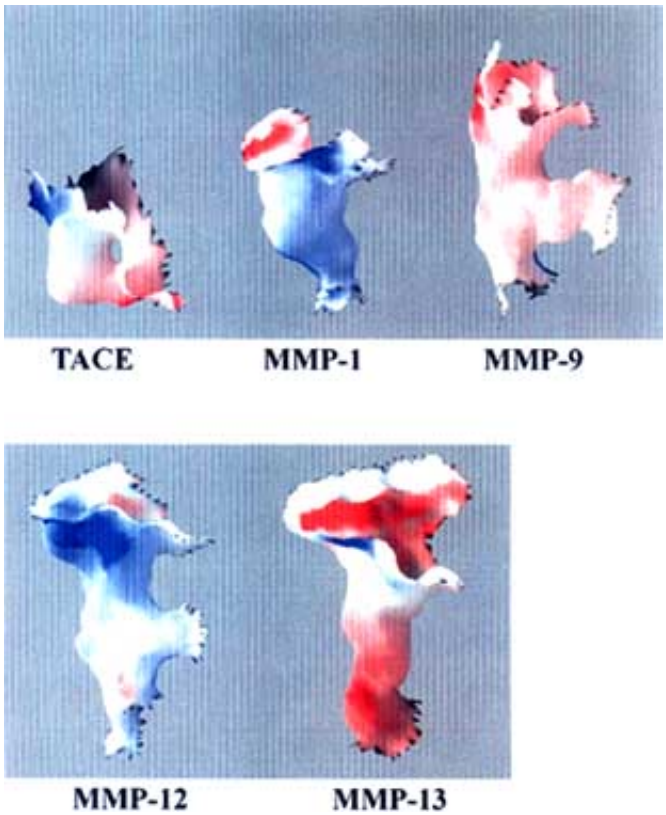

Fig. (5). GRASP surface of the S1' pocket for TACE, MMP-1, MMP-9, MMP-12 and MMP-13. Blue and red indicate positively charged and negatively charged surfaces, respectively. The surfaces are all oriented such that the active site zinc is at the top left, and the specificity loop at the bottom.

of the L81-N80 amide bond, thus making the amide NH an even better hydrogen bond donor. Consequently, a significant number of hydrogen bond interactions have been observed between inhibitors and MMP-1 in this kinked region [37-40], and it is presumed that this optimized hydrogen bonding network helps drive the binding and catalysis of the native collagen substrate [41].

A major feature of the MMP-1 active site is its hydrophobic S1' pocket with a positively charged surface at the bottom due to the capping of the pocket by R114 (Figs.

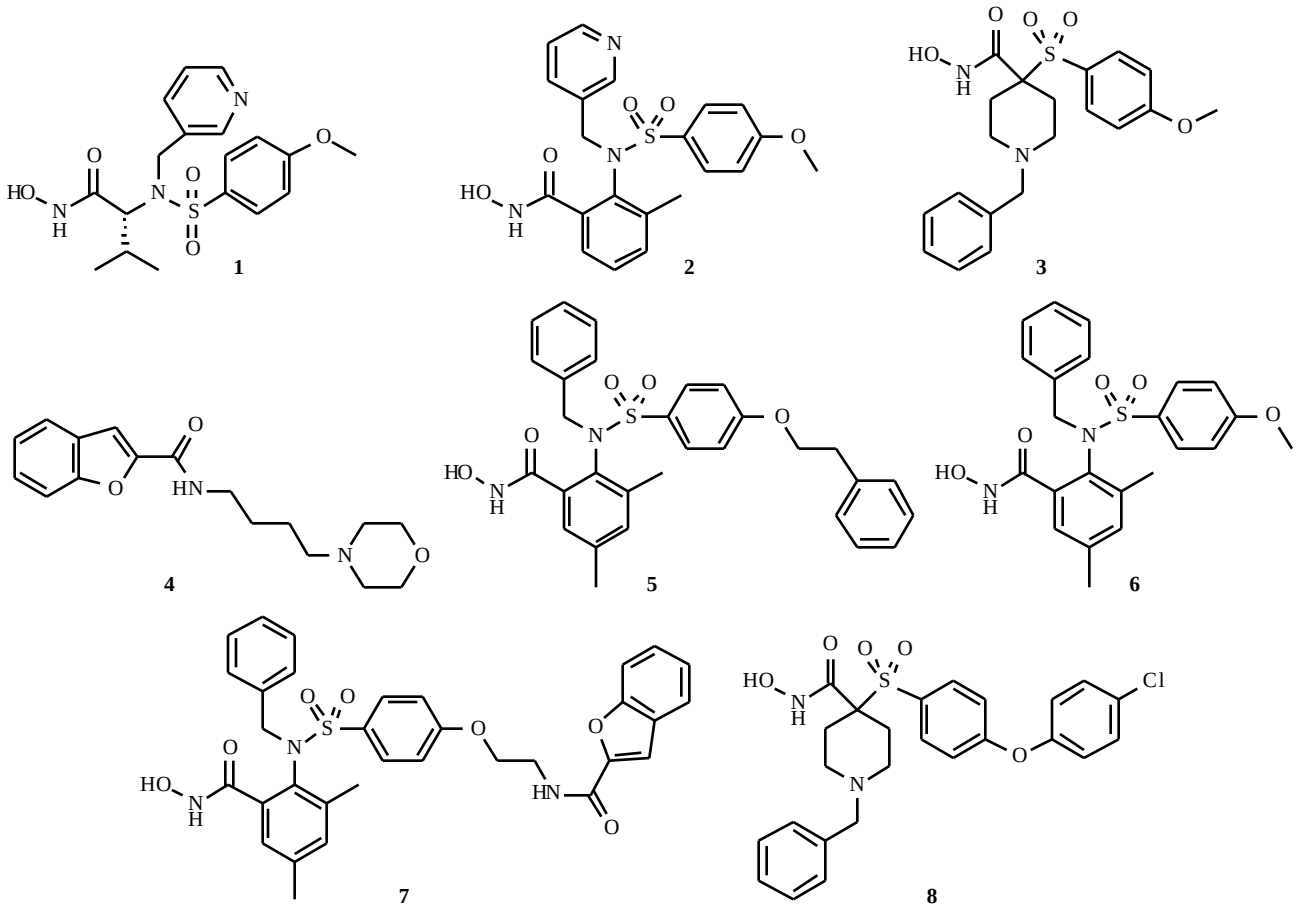

Fig. (6). Chemical structures of MMP inhibitors.

(**3**) and (**5**)) [36]. There are two additional regions of positive charge at this site, corresponding to the area of the catalytic zinc, and to the protein backbone of residues A82 and L81**.** Also, the side-chain of N80 occupies the active site and partially blocks access to the S1' pocket in the free form of the enzyme. Consequently, the size and depth of the MMP-1 S1' pocket is relatively small and shallow compared to other MMPs. This highlights a recurring theme when comparisons are made between the MMP structures. That is, the size, shape and amino acid composition of the S1' pockets are the major structural differences between the enzymes. It is important to note, however, that the sidechain of R114 has been observed to move, which in combination with the mobility of the active site loop, moderately increases the effective size of MMP-1's S1' pocket [23].

Contrary to MMP-1, which can be stable in the absence of an inhibitor for a few months at millimolar concentrations, MMP-13 exhibits significant degradation within an hour, even at dilute concentration (50 μM). This autocatalytic behavior necessitates that all structural work on MMP-13 be done in the presence of an inhibitor. Therefore, in our studies, NMR and X-ray structures were obtained for MMP-13 complexed with compound **2** (Fig. (**6**)). The atomic root mean square deviation (RMSD) for residues 7-164 between the minimized mean NMR structure and the X-ray structure is 1.49 Å for the backbone atoms, indicating that the structures are virtually identical [42,43]. The majority of the differences between the NMR and X-ray structures appear to be associated with loop dynamics. The largest difference occurs in the loop region containing the structural zinc binding site (residues 66-75) which is "pushed-up" relative to the MMP-13 X-ray structure. Similarly, the overall fold of MMP-13 is essentially identical to MMP-1 and other MMP structures (Fig. (**4**)). This is clearly evident from the 1.95 Å RMSD obtained for the best-fit superposition of the backbone atoms from the NMR structures of inhibitor-free MMP-1 and MMP-13 complexed to **2**. The inherent similarity in the MMP catalytic domains was further illustrated by the utility of an MMP-13 homology model based on the MMP-1 NMR structure for the initial analysis of MMP-13 NOESY data [43].

A high sequence similarity exists between MMP-1 and MMP-13 in the active site (Figs. (**2**) and (**7**)). However, while there are only a few significant residue differences between MMP-1 and MMP-13, these modifications result in a significant change in the local environment of the active site. For example, the R114 (MMP-1) to L115 (MMP-13) "substitution" in the S1' pocket essentially converts a short, polar cavity into a long hydrophobic one, as depicted in Fig. (**5**). Another example is the N80 (MMP-1) to L81 (MMP-13) substitution near S2', which gives MMP-13 a more sterically crowded, hydrophobic pocket as compared to a more open, hydrophilic S2' environment for MMP-1. A

similar change occurs in the active loop region, where I140, a bulky hydrophobic residue in MMP-13, replaces the smaller hydrophilic S139 residue in MMP-1.

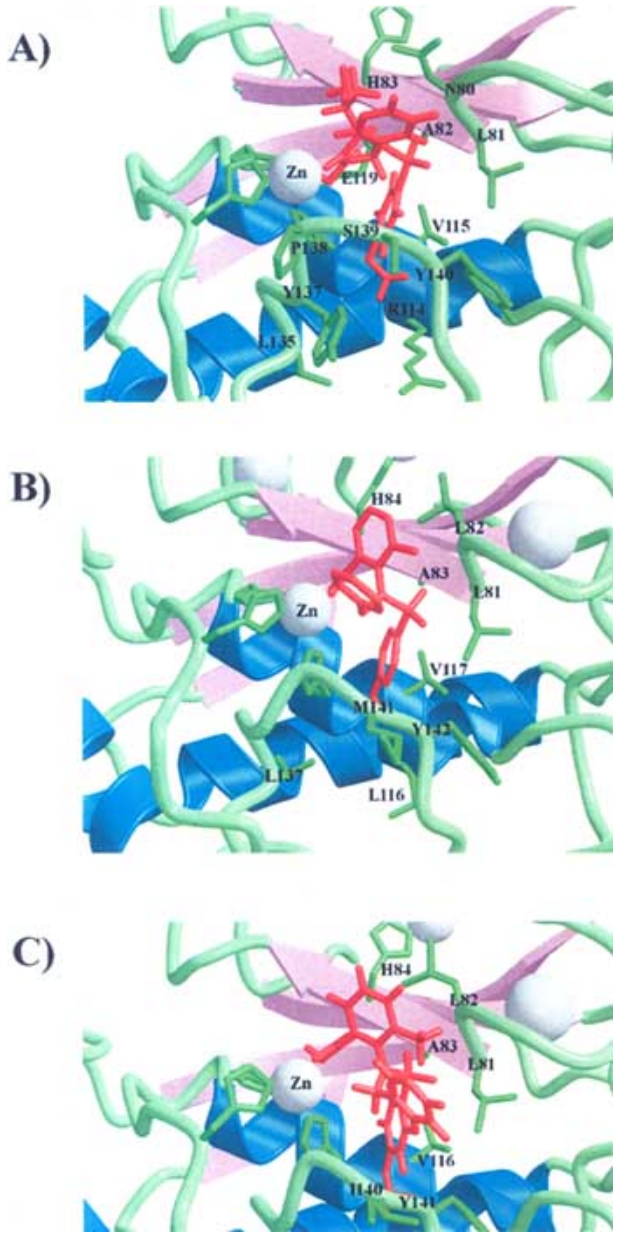

Fig. (7). Expanded ribbon diagram of the MMP active-site for the (a) MMP-1: compound **2**, (b) MMP-9: compound **1** and (c) MMP-13: compound **1** complexes. Side-chains (green) for residues involved in the interaction with the inhibitor (red) are shown and labeled.

It is prudent to again stress the point that the most striking structural difference between MMP-1 and MMP-13 is the relative size and shape of the S1' pocket (Fig. (**5**)). The S1' pocket for MMP-13 nearly reaches the outer surface of the protein and is greater than twice the size of the pocket in MMP-1. This very prominent difference immediately suggested that a means for designing in specificity for MMP-13 would be to take advantage of the filling capacity of this pocket.

Determining X-ray structures for MMP-9, MMP-12 and TACE extended this structural comparison by cataloguing the variety of S1' shapes and sizes (Fig. (**5**)). A comparative analysis of the MMP structures shows that in general residue positions 115 and 144 (based on the MMP-13 sequence numbering), in addition to the length of the specificity loop, effectively determines the size and shape of these S1' pockets. The larger the side chains at positions 115 and 144 results in a smaller S1' pocket. Since residue 115 is spatially closer to the catalytic zinc, a larger side chain at this position will have a greater impact on defining a smaller S1' pocket relative to the residue type at position 144. MMP-1 has the largest side chain at position 115, thus its S1' pocket is the smallest. MMP-13 has short side chains at both positions 115 and 144. This combined with an increase in length of its specificity loop result in MMP-13 having the largest S1' pocket. MMP-9 falls between MMP-1 and MMP-13 since it has an Arg at position 144, a Leu at position 115, and a specificity loop length equivalent to MMP-1. The S1' subsite of MMP-12 is also similar in size and shape to that of MMP-13, as it has a leucine at position 115, a lysine at position 144, and a similar sized specificity loop.

While TACE is not a member of the MMP family, its zinc-dependent endopeptidase activity also warrants comparison in the development of MMP specific inhibitors [44]. This is supported by the ability of many MMP inhibitors to potently inhibit TACE [45]. An examination of the TACE structure can provide insights into eliminating non-specific binding of MMP inhibitors to general zinc-containing enzymes and can also allow the design of TACE specific inhibitors.

The TACE structure is relatively larger than the consensus MMP structure and contains an additional helix and a multiple-turn loop segment [44]. Also, the TACE structure lacks the structural zinc and calcium seen in the MMPs. Despite a low sequence homology and divergent structural elements, the TACE and MMP structures do contain some common features as evidenced by the 1.6 Å RMSD between 120 topologically equivalent C-α atoms. More importantly, the active site of TACE is reminiscent of the MMPs. The TACE active site contains the conserved zinc-binding motif (HExxHxxGxxH), where the histidines that coordinate the zinc are in the active-site helix and the specificity loop. Similar to the MMPs, TACE contains three flat substrate subsites to the left of the catalytic zinc (unprimed sites), and three deep subsites to the right (primed subsites) (Fig. (**3**)). An interesting feature of the TACE active site is the structure of the S1' and S3' pockets (Figs. (**5**) and (**13**)). The two pockets have effectively merged and created an "L-shaped" S1' binding cleft that opens up into the S3' pocket. Access to the S3' pocket is partially obscured by the opposing side-chains of A439 and L348. The S1' pocket is medium-size and both S1' and S3' are hydrophobic, connected by a polar entrance. Clearly, the characteristics of the TACE binding pocket are unique relative to MMP-1, MMP-9 and MMP-13, and therefore, TACE is exceptionally amenable to specificity-driven structure-based design.

MMP ACTIVE SITE DYNAMICS

The availability of the MMP structures provides an initial framework for the design of high-affinity and specific inhibitors. However, a complicating factor to the general structure-based drug design approach was the unexpected observation of extensive mobility in the MMP active site. MMP active site dynamics were initially observed in the NMR structure of inhibitor-free MMP-1 [34,35]. On the contrary, prior X-ray structures of MMP-1 complexed to inhibitors exhibited relatively low B-factors for the active site residues, which are not suggestive of mobility [39,40]. The lack of a correlation between B-factors from X-ray structures and protein mobility is not an uncommon occurrence [46-51].

The active site mobility for inhibitor-free MMP-1 was evident from measured generalized order parameter (S^2), peak multiplicity and weak or missing peaks (Fig. (**8**)). A number of residues that comprise the MMP-1 active site appear as doublets in the ^1H-^{15}N HSQC spectra that disappear in the presence of an inhibitor. The observed doublets in the ^1H-^{15}N HSQC spectra might be the result of a slow conformational change in the active site that results in a concerted motion of helix B (L112-S123), the zinc-ligated histidines (H118, H122, H128) and the nearby loop region. The presence of an inhibitor that binds by chelating the zinc effectively removes this motion while maximizing the inhibitors interaction with β-strand IV. The mobility of the active site is further exemplified by the observation that residues F142 to G144 did not exhibit a cross-peak in the ^1H-^{15}N HSQC spectra, and that residues P138 to G144 are poorly defined in the structure based on the lack of information in the ^{15}N-edited NOESY spectra. In the presence of an inhibitor, this region is still poorly defined, and the only new cross-peak observed in the ^1H-^{15}N HSQC spectra of the complex is for G144. This indicates a lack of an interaction and no significant change in the mobility for residues P138 to G144 (Figs. (**7**) and (**8**)).

The generalized order parameters (S^2) determined from ^{15}N T_1, T_2 and NOE data for free and inhibited MMP-1 further established the mobility of the MMP active site. The average values of the order parameter S^2 for free MMP-1 and inhibited MMP-1 are 0.89 ± 0.06 and 0.88 ± 0.05 respectively, indicating a limited conformational flexibility for most of the protein. In contrast, residues P138 to G144 are highly mobile in both the free and inhibited MMP-1 samples with order parameters (S^2) ≤ 0.6. This also indicates that the inhibitor does not affect the dynamics of this loop region suggesting that the interaction with the P138-G144 loop is not crucial for binding to the protein.

These results indicate that the inhibitor free active site of MMP-1 is significantly more mobile than was implied from the original X-ray structures of MMP-1 in the presence of an inhibitor. In particular, it suggests that helix B and the ligated zinc may be in a slow conformational exchange, and that the random coil region in the vicinity of the active site

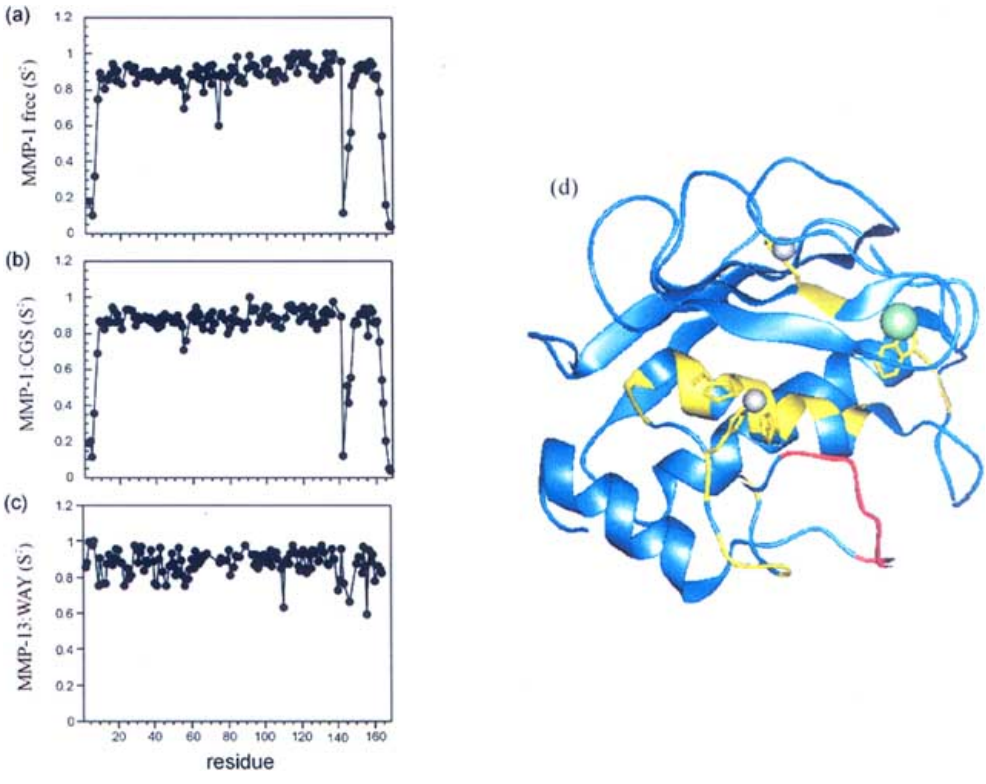

Fig. (8). MMP active site dynamics. Per residue plot of the order parameters (S^2) for (a) MMP-1 free, (b) MMP-1 complexed with **2** and (c) MMP-13 complexed with **1** illustrating the mobility of the MMP active site and the effect of inhibitors on the mobility. (d) Ribbon diagram of MMP-with residues exhibiting doubling of peaks in the ^1H-^{15}NHSQC colored yellow, which indicates slow exchange, and the mobile active site loop is colored red. (Reprinted from reference 34, Copyright 2000, with kind permission from by Kluwer Academic Publishers).

has a high order of mobility to the extent that the NHs for F142 to G144 are broadened beyond detection.

Subsequent to our initial dynamics analysis of MMP-1, additional data has been obtained that substantiates the general mobility of MMP active sites and its impact on drug design [23,43,52-54]. Similar NMR dynamic studies have indicated comparable mobility in the active-site loop for both MMP-3 [52] and MMP-13 [43,53] (Fig. (**8**)). The extent of the active site mobility was dependent on the nature of the bound inhibitor and the particulars of the inhibitor's interaction with the MMP. In general, the mobility of the active site loop may be decreased by beneficial binding interactions between the inhibitor and the protein, but residual flexibility relative to the remainder of the protein is persistent. This observation is consistent with early X-ray structures that exhibited low B-factors for the active site loop, which were comparable to the remainder of the protein. A potential source of the decreased mobility may be the inhibitor's ability to extend the formation of a β-sheet between β-strand IV and the disordered residues corresponding to the active site loop region. This particular mechanism is prevalent in peptide mimetic inhibitors.

A consequence of the active site loop mobility is a relative elasticity of the active site, particularly in the primed subsites. The impact on drug design was clearly illustrated in MMP X-ray structures that demonstrated the ability of side chains in the active site to undergo conformational changes to accommodate a bound inhibitor [23]. Effectively, a compound predicted to have poor inhibition activity against a MMP based on a poor fit in the S1' pocket may be accommodated in the binding site due to the protein's mobility. Further complicating the design endeavor has been the observation that inhibitor dynamics may augment the protein's mobility, permitting a compound predicted to have poor steric interactions to bind the MMP with high affinity [54] (Fig. (**9**)). Clearly, the observed mobility of the MMP active site complicates the design of potentially selective inhibitors.

MMP STRUCTURE-BASED INHIBITOR DESIGN

X-ray, NMR and molecular modeling have played an important role in the development of potent and selective MMP inhibitors. The availability of the MMP catalytic domain structures described above provides the necessary framework for the further design of high affinity and selective MMP ligands. While MMP inhibitors fall into a number of chemical classes (e.g. anthranilic acids, sulfones, sulfoxides, and sulfonamides), common features among them target chemical features of the enzyme active site that are known to be important for its function as a protease. These include a zinc chelating functionality (e.g. hydroxamic acid, carboxylic acid, thiol, phosphate), hydrogen bond acceptors to interact with residues within β_{IV}, and a hydrophobic P1' chemical moiety that fits snugly into the S1' pocket. The most potent inhibitors typically contain a hydroxamic acid zinc chelating functionality. Analysis of the affinity of these inhibitors suggests that most of the binding energy arises from an efficient chelation of the active site zinc and hydrogen bond interactions with several nearby residues, including the catalytic glutamate. Conversely, selectivity appears to be manifested by the fit in the relatively deep S1' pocket and to a lesser extent the S2' pocket. A prevalence of MMP inhibitor design has focused on achieving selectivity for a specific MMP based on this general outline, while maintaining potent binding through active site hydrogen bonds and zinc chelation.

Concurrent with the NMR and X-ray structures of the various MMPs has been the structural information obtained for a variety of MMP inhibitors [5]. Structures for some of the inhibitors have been determined in multiple MMPs, permitting a direct comparison and evaluation of the different binding interactions across related binding sites (Fig. (**7**)). In our laboratories, a number of MMP inhibitor complexes have been determined using both NMR and X-ray techniques, where again, our primary interests lie with MMP-1 and MMP-13.

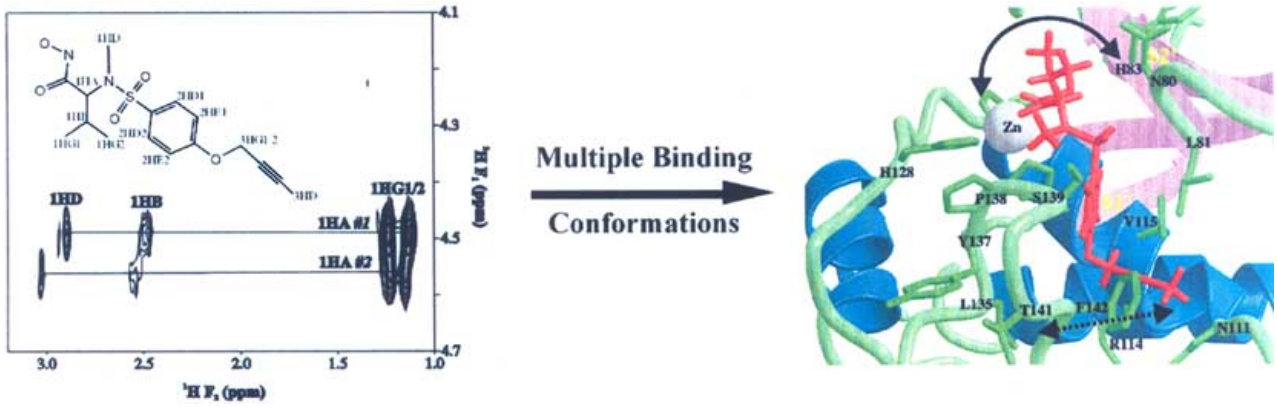

Fig. (9). (left) Expanded region of the 2D-12C,12C-filtered NOESY experiment for compound **10** complexed to MMP-1. (right) Ribbon diagram of one potential conformation of the MMP-1: compound **10** complex, where the solid arrow indicates the rocking motion associated with the slow-exchange and the dashed arrow indicates the fast-exchange "twist" motion of the butynyl group pocket. Side-chains (green) for residues involved in the interaction with compound **10** (red) are shown and labeled. (Reprinted with permission from reference 54, Copyright 2000 by American Chemical Society).

In the case of NMR, MMP-inhibitor complexes have been determined utilizing two approaches: direct determination of the high-resolution solution structure of the MMP-inhibitor complex or a structure based on merged NMR data [36]. The determination of a high-resolution structure of a protein or protein-ligand complex by NMR is a very arduous task requiring on average 6 months to a year to complete [55,56]. The majority of this effort is dedicated to the manual analysis of NOESY spectra to obtain assignments for distance constraints. Clearly, this typical timeframe is inadequate as part of a structure-based drug design program that requires a constant supply of structures during the iterative design process [57-60]. To compensate for this problem, the majority of the protein-ligand complexes determined by NMR utilized a merged data set approach [36].

The refinement of additional MMP-1 and MMP-13 inhibitor complexes were based on distance and dihedral restraints determined for the high-resolution solution structure of inhibitor-free MMP-1 [34,35] and the MMP-13: compound **2** [42,43] complexes appended with the intra and intermolecular NOEs from the new inhibitor complex. The inhibitor-free MMP-1 and MMP-13: compound **2** NMR restraints were modified as appropriate for residues in the vicinity of the active site by either removing restraints inconsistent with the new MMP inhibitor structure and/or by the addition of new restraints observed in the complex. Inhibitor-free MMP-1 or MMP-13: compound **2** NMR restraints were identified as inconsistent with the new MMP inhibitor structure when the restraint was consistently violated in structures calculated for the complex. Since the restraints from the reference structures did not exhibit any distance violations greater than 0.1 Å or dihedral angle violations greater than 1°, any observed violation with the new MMP inhibitor structure was inherently incompatible with the new complex. This technique effectively filters-out any bias in the structure determination process for the complex by giving the NOEs observed for the new MMP-inhibitor complex absolute precedent over the prior restraints. This method permitted the structure of the active site to be determined primarily by the observed intermolecular NOEs between the MMP and the new inhibitor, and the inhibitor's intramolecular NOEs. The remainder of the protein is predominantly defined by the original inhibitor-free MMP-1 and MMP-13:compound **2** restraints.

For MMP-inhibitor structures determined using X-ray crystallography, typical crystallization, data collection and refinement techniques were applied.

CGS-27023A Complexed to MMP-1, MMP-3 and MMP-13

The first reported structural information for a non-peptidic small molecule bound to an MMP was presented in an NMR structure of **1** complexed with MMP-3 [61,62]. This structure revealed the nature of the interaction of the small molecule with the protein, and the detailed positioning of the individual functional groups. Since then, X-ray and NMR structures have also been reported for this molecule in complex with MMP-1 [36] and MMP-13 [53], helping further the design of selective inhibitors.

The important details of the interaction revealed in the MMP-3 complex included the positioning and protonation state of the hydroxamic acid functionality, the presence of hydrogen bonds between the inhibitor and protein, and the location of the methoxyphenyl moiety within the active site (Fig. (**10**)). Most importantly, it was revealed that the hydroxamic acid functionality was playing a major role in the interaction of this molecule with the protein. Not only were the two oxygen atoms interacting directly with the catalytic zinc, but also both the NH hydrogen and the hydrogen of the protonated sp^3 oxygen were interacting with the protein through the backbone carbonyl of A82 and the sidechain of E119, respectively. Another important enthalpic interaction was the hydrogen bond between one of the sulfonamide oxygens and the backbone NH of L81. The kink in the backbone at this position in the protein chain forms the aforementioned "hot spot" for hydrogen bond acceptors; two backbone NH's point to the same region of space and are likely to have a role in promoting proteolysis of the natural substrate (Fig. (**3**)). The methoxyphenyl group was found to occupy the S1' substrate pocket, where binding is likely to be afforded by a π-stacking interaction with a nearby histidine, van der Waals interactions with protein atoms in the pocket, and the hydrophobic effect.

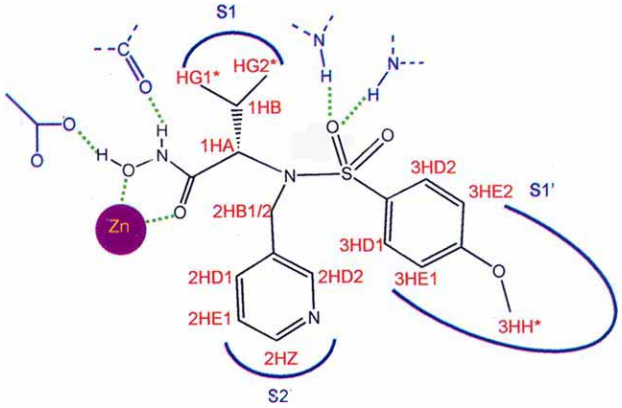

Fig. (10). A schematic 2-D representation of **1** bound to MMP-3.

Comparison of the binding mode of this compound across MMP-1, MMP-3 and MMP-13 illustrates some important differences between MMPs in general, and how these differences can be used to build in inhibitor selectivity. First and foremost, there is a large difference in the size of the S1' pocket between MMP-1, MMP-3 and MMP-13 (see Fig. (**5**) for a comparison of MMP-1 and MMP-13). Compound **1** effectively fills the available S1' pocket for MMP-1, but there is additional space available in the MMP-3 and MMP-13 S1' pockets. In addition, **1** fits deeper in the S1' pocket for MMP-13 relative to MMP-3 and MMP-1. Comparison of **1** bound to MMP-1 and MMP-3 indicates that there are only two MMP-1 residues, N80→V and R114→L that are involved in direct interaction with **1** that are distinct in the MMP-3 active site. Similarly, comparison between MMP-1 and MMP-13 identified residues (N80→L, R114→L and S139→I) that are involved in direct interaction with **1**, and that are distinct in the MMP-13 active site.

Overall, the conformation of **1** is similar in MMP-1, MMP-3 and MMP-13. However, the NMR data for these complexes suggest some subtle differences between the

binding of **1** to these proteins. The most important difference is the distinct intramolecular NOEs observed for **1** in the complexes. In MMP-1, NOEs are seen from HG1* to both 2HE1 and 2HZ. These NOEs are not observed in the spectra of the other complexes. Conversely, NOEs between 3HD2 and 2HD1/2HD2 are observed in the MMP-3 and MMP-13 complex but not in the MMP-1 complex**.** Additionally, an NOE between 1HB and 2HD2 is only observed in the MMP-13 complex structure resulting in an eclipsed orientation of the pyridine ring with the isopropyl group. This may result from the deeper penetration of **1** in the MMP-13 S1' pocket and a narrow fit in the S1 and S2' pocket. These observations suggest a stronger interaction of the isopropyl group with the pyridine ring in the MMP-1 complex as opposed to a stronger interaction between the p-methoxyphenyl group and the pyridine ring in the MMP-3 and MMP-13 complexes.

Similarly, there are differences in the observed intermolecular NOEs between inhibitor **1** and MMP-1, MMP-3 and MMP-13. In MMP-1, NOEs are observed between the isopropyl methyls and the backbone and side-chain atoms of N80 and H83, while the backbone and side-chain atoms of A82 interact with the p-methoxyphenyl group. Conversely, in MMP-3 and MMP-13, A82 interacts with the isopropyl methyl group in addition to the p-methoxyphenyl group. Furthermore, an NOE is seen between the pyridine ring and L81 in MMP-3 and MMP-13, but the only NOEs to the pyridine ring in MMP-1 are to P138 and S139.

These differences suggest a distinct orientation in the positioning of **1** relative to βIV for MMP-1 compared to MMP-3 and MMP-13. This subtle difference in the orientation of **1** can probably be attributed to the sequence difference between MMP-1 and both MMP-3 and MMP-13. Thus, N80 in MMP-1 is replaced by either a valine or a leucine in MMP-3 and MMP-13, respectively. It appears that the bulkier leucine/valine side-chains may rotate the isopropyl group and the pyridine ring closer to βIV as evidenced by the NOEs to A82 and L81, respectively. Additionally, the hydrophobic Leu/Val side-chains probably provide a better interaction with the isopropyl and pyridine ring than the polar N80 side-chain.

Anthranilate Hydroxamate 2 Complexed to MMP-9 and MMP-13

Another starting point for the design of potent and selective MMP-13 inhibitors is **2**, an anthranilate sulfonamide hydroxamic acid (Fig. (**6**)) [63]. The X-ray and NMR structures of this molecule bound to MMP-13 revealed a binding mode similar to the one observed for **1** (Figs. (**7**) and (**10**)); the hydroxamate chelates the zinc, a sulfonamide oxygen hydrogen bonds to the protein backbone, and the methoxyphenyl moiety occupies the S1' pocket of the active site.

A comparison of the X-ray structure of **2** complexed to MMP-9 with the NMR structure of the MMP-13:compound **2** complex [43] exemplifies an inherent difficulty in obtaining inhibitor specificity for a particular MMP. The overall structure and details of the active site between MMP-9 and MMP-13 are very similar (Figs. (**2**), (**4**), (**5**) and (**7**)). This is clearly illustrated by the nature of the side-chains that directly interact with **2**. Nine amino acids from MMP-9 and MMP-13 make critical interactions with **2**. Of these nine residues, eight are identical between MMP-9 and MMP-13. The sole difference is the minor substitution of I140→M between MMP-13 and MMP-9, respectively. Further minimizing the impact of this amino acid change is its location in the dynamic active site loop region. As a result, the binding conformation of **2** in the MMP-9 and MMP-13 binding site are essentially identical. This is further exemplified by the identical binding affinity of **2** to MMP-9 (IC_{50} = 34 nM) and MMP-13 (IC_{50} = 33 nM). Consequently, identifying and designing an inhibitor selective for MMP-13-over MMP-9, or the reverse, has been a challenging endeavor. Nevertheless, a potential route to inhibitor selectivity between MMP-9 and MMP-13 may occur through further exploitation of the size, shape and chemical differences deep in the S1' pocket (Figs. (**2**) and (**5**)). While the residues involved in the direct interaction with **2** are effectively identical, there are other amino acid changes that affect the relative size and shape of the S1' pocket. MMP-13 contains a two amino acid insert in the dynamic active site loop (S147 and H148). Similarly, MMP-9 contains an amino acid insert in the loop region following helix α_B (D109). The result is a longer and more linear S1' pocket for MMP-13 relative to MMP-9. Also, MMP-9 contains a bulge in its S1' pocket. In fact, we were successful in exploiting this difference in the MMP-9 and MMP-13 S1' pocket by designing a novel inhibitor specific for MMP-13 that we describe in detail later in this review.

A major distinction between the MMP-13:compound **2** and MMP-1:compound **1** structures is the change in MMP mobility (Fig. (**8**)). The dynamic analysis of inhibitor-free MMP-1 and MMP-1 complexed to **1** indicated no change in the mobile active site loop upon inhibitor binding, as is evident from the consistent order parameters (S^2). This lack of a mobility change suggests the absence of any significant binding interaction between **1** and the mobile loop region. Conversely, the mobility of the corresponding loop region in MMP-13 has been reduced, relative to MMP-1, in the presence of **2**. This mobility change may result from the S139→I residue difference between MMP-1 and MMP-13. In the MMP-1:compound **1** structure, the pyridine ring position is essentially undefined and solvent exposed. In the MMP-13:compound **2** structure, the pyridine ring interacts with the side-chain of I140. Clearly, isoleucine is a bulkier, more hydrophobic group relative to serine that provides a beneficial hydrophobic interaction with the pyridine ring of **2**. This positive binding interaction probably contributes to the decreased loop mobility. It is important to note, that while the relative mobility of the loop region has decreased in the presence of **2**, the active-site loop is still more mobile compared to the remainder of the core MMP-13 structure.

Compound 4 Complexed to MMP-13

A break-though in obtaining selectivity against other MMP's of interest was afforded by the discovery of **4**, a high-throughput screening hit [64]. Although **4** was found to be a modest inhibitor of MMP-13 (IC_{50} = 3.2 μM) it

appeared to be almost purely MMP-13 selective, with no apparent activity against MMP-1, MMP-9, and TACE.

Interestingly, the chemical structure of **4** does not contain an obvious zinc chelating substituent, so its binding interaction with the MMPs could not be readily predicted. Carboxamide **4** is a linear, flexible molecule containing a morpholine group at one end and a benzofuran at the other. This is consistent with the size and shape of the S1' pocket for MMP-13 which is very deep and linear while nearly reaching the surface of the protein. Property analysis of the S1' pocket indicates that the end adjacent to the zinc is relatively polar whereas the opposite end is hydrophobic, consistent with the characteristics of the morpholine and benzofuran groups, respectively. The NMR structure of the MMP-13: compound **4** complex revealed that **4** sits deep within the MMP-13 S1' pocket with the morpholine ring adjacent to the catalytic zinc and the benzofuran group sitting in a hydrophobic pocket formed by L115, L136, F149 and P152 at the base of the S1' pocket (Fig. (**11**)). The morpholine oxygen forms a hydrogen bond with the backbone amide group of L82 and the peptide bond linker forms hydrogen bonds with MMP-13 backbone groups.

Subsequent computational analyses of the NMR structure revealed the major contributors to its ΔG of binding, and consequently helped to guide the further evolution of **4** into a potent and selective inhibitor of MMP-13. Factors that are favorable to the binding of **4** include the hydrophobic effect (loss area of ~ 880 A^2), van der Waals interactions, and the well-shielded hydrogen bonds between the amide functionality of the inhibitor and the backbone atoms. In contrast, unfavorable contributions to binding are the stretch of unencumbered rotatable bonds and amide desolvation costs for the ligand, as well as the protein's desolvation costs (mostly S1' backbone carbonyls).

The availability of this analysis provided a clear approach towards achieving a potent and selective molecule by adding a more rigid, zinc chelating functionality to the morpholine end of the molecule. This would maintain the favorable binding interactions and selectivity profile of **4**, while obtaining substantial binding energy from the conserved region of the binding site. Anthranilate hydroxamates such as **5** [65] and **6** were chosen as scaffolds for this purpose. Using the available experimental structures and structure-based molecular modeling techniques [64] a hybrid inhibitor (**7**) was thus designed (Fig. (**11**)). When tested against several other zinc-endopeptidases, **7** exhibited an IC_{50} of 17 nM against MMP-13, and was >5800, 56 and >500 fold selective over MMP-1, MMP-9 and TACE respectively. In each case, the selectivity is afforded by the depth of penetration into the S1' pocket, and the chemical environment at the base of the pocket. As mentioned previously, MMP-13 has the deepest, most linear, and most hydrophobic S1' pocket**.** None of the other enzymes have the ability to accommodate the amide-benzofuran moiety in the same manner in this cavity.

Sulfone Hydroxamate 3 Complexed to MMP-13

A closely related series of molecules pursued in our MMP-13 inhibitor program is exemplified by **3**, in which one atom separates the sulfone and hydroxamic acid groups [66]. Interestingly, the small difference in the molecular makeup of the "head piece" of these molecules typically afforded better selectivity over MMP-1, as well as better *in vivo* properties. For example, **3** exhibits IC_{50}s of 2 nM and 492 nM against MMP-13 and MMP-1, respectively. The X-ray structure of **3** bound to MMP-13 revealed that the shorter link between the hydroxamic acid and sulfone group forced the molecule to bind with a slightly different orientation relative to **1** and **2** that promotes selectivity over MMP-1.

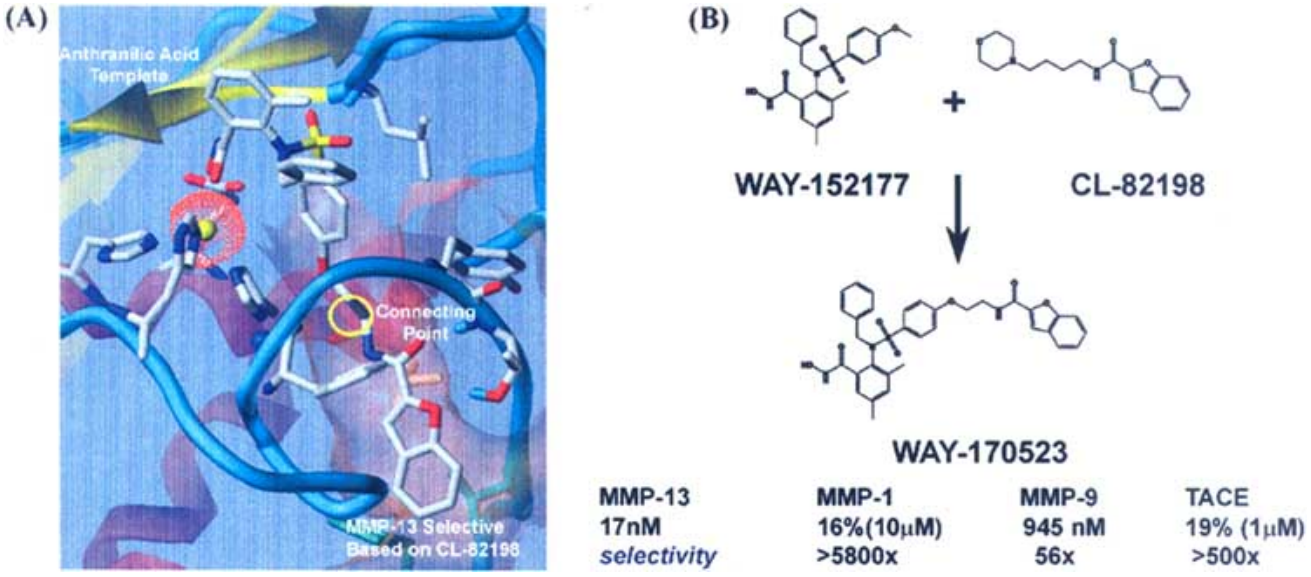

Fig. (11). (A) Expanded view of the NMR MMP-13: compound **6** complex overlayed with the MMP-13: compound **4** model demonstrating approach to forming the hybrid inhibitor **7**. (B) Design scheme showing the flow from **4** and **6** to **7**, and a table listing the observed IC_{50}'s for the hybrid compound. (Reprinted with permission from reference 64, Copyright 2000 by American Chemical Society).

Since the enthalpy of the hydroxamic acid interaction with the active site zinc is greater than the sulfone hydrogen bond with the NH of L81, the sulfone is forced closer to the active site zinc. This movement of the sulfone places the hydrogen bond accepting oxygen midway between the backbone NH of L81 and A82 (the aforementioned active site "hotspot"). The ring system extending from the atom connecting the hydroxamic acid and the sulfone groups is thereby firmly placed over the hydrophobic sidechain of L80 in MMP-13. As discussed above, a polar asparagine residue replaces L80 in MMP-1, which probably accounts for the diminished affinity of **3** against MMP-1.

Compound 8 Complexed to MMP-13

One of the next design iterations in the series including **3** was to extend the P1' group of the inhibitor to reach further down into the MMP-13 S1' subsite to capitalize on the size, shape and chemical differences of the pocket (Fig. (**5**)). As mentioned above, the steric hindrances presented by the smaller S1' pockets in the other MMPs relative to MMP-13 should further increase compound selectivity. This in fact was the case for **8**, an analog of **3**, with a biaryl ether P1' substituent [66]. Compound **8** has IC_{50}s of 0.9 nM and 801 nM against MMP-13 and MMP-1, respectively. The crystal structure of MMP-13 complexed with **8** confirmed that the additional phenyl ring extends deep into the hydrophobic region of the S1' pocket.

INHIBITORS OF TACE

In the pursuit of agents for the treatment of rheumatoid arthritis, compounds with increased potency against TACE were highly desirable. The generation of a TACE homology model had led to the design of inhibitors bearing a butynyloxy P1' group that could fit optimally in the enzyme S1' pocket and the space linking it to the S3' subsite [67-70]. Two such analogs will be discussed, one based on an α-amino hydroxamate [70] and a second related to a bicyclic heteroaryl scaffold [69] (Fig. (**12**)).

Compound 9 Complexed to TACE

The structure of **9** bound to TACE revealed that the butynyl tail of the molecule beautifully nestles itself into the narrow tunnel connecting the S1' and S3' pockets (described above), while the hydroxamate-sulfonamide portion of the molecule interacts with the protein as it does with the other zinc-metalloproteases (Fig. (**13**)). The strong hydrophobic/ contact nature of the former interaction, plus the typical hydrogen bonds of the sulfonamide and hydroxamate, and zinc chelation, endows **9** with an IC_{50} of 4 nM in a TACE *in vitro* peptide-cleavage assay. Its activities against MMP-1, MMP-9 and MMP-13, however, are 4.0 μM, 796 nM and 195 nM, respectively.

Given the flexibility of the molecule around the tail's ether functionality, it is not surprising that **9** also inhibits MMP-9 and MMP-13, even though the shapes of their S1' pockets are drastically different. However, it is interesting to note that compound **10** (TACE IC_{50} = 15 nM), the closely related N-methyl sulfonamide analog of compound **9**, is 100-fold more potent against MMP-1 than compound **9**. Thus, it exhibits an MMP-1 IC_{50} of 259 nM while **9** has an IC_{50} of 4 μM. This is most likely due to the fact that **9** is an NH sulfonamide, while **10** is an N-methyl sulfonamide. Molecule flexibility is likely to play a major role in differentiating the activities, while desolvation costs and van der Waals interactions may play more minor but additive roles.

As previously alluded to, the inherent flexibility of the MMP active site and potential elasticity of the S1' pocket upon ligand binding complicate the inhibitor design process. This problem is clearly illustrated in recent MMP X-ray structures which demonstrates the ability of side chains in the active site to undergo conformational changes and accommodate a bound inhibitor that was not predicted to fit based on prior structures [5,23]. The design of inhibitor **10** [70] is a further example of the difficulties and unexpected outcomes that arise as a result of dynamics. In addition to the mobility of the active site of MMP-1, compound **10** also exhibits conformational exchange to compensate for a suboptimal fit in the S1' pocket (Fig. (**9**)). The binding of **10** to MMP-1 overcomes the steric clash and poor fit of the butynyl group in the MMP-1 S1' pocket by maintaining a significant entropic contribution to its free energy of binding, and through the elastic nature of the MMP active site. This is accomplished by a rapid twisting motion of the butynyl group between two reasonable binding modes in the S1' pocket, an apparent slow "rocking" motion of the isopropyl group about the catalytic zinc, and the active site loop and side chain motions observed in prior structures [23,34,35,43,53]. The interchange between the various conformers maintains positive interactions with the MMP-1 active site resulting in the observed low nanomolar affinity. In effect, the intrinsic energetic cost of opening the S1' pocket to accommodate **10** is partially compensated for by the motions exhibited by the compound in the complex. These results with compound **10** indicate that the contribution of both MMP and inhibitor dynamics can complicate the design effort, and that static models may

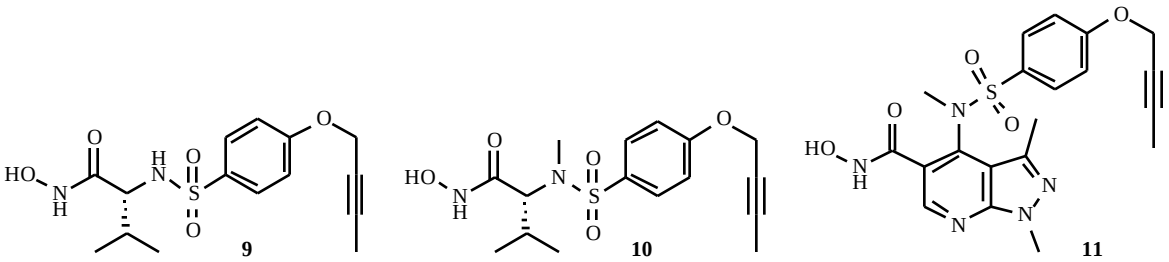

Fig. (12). Chemical structures of TACE inhibitors.

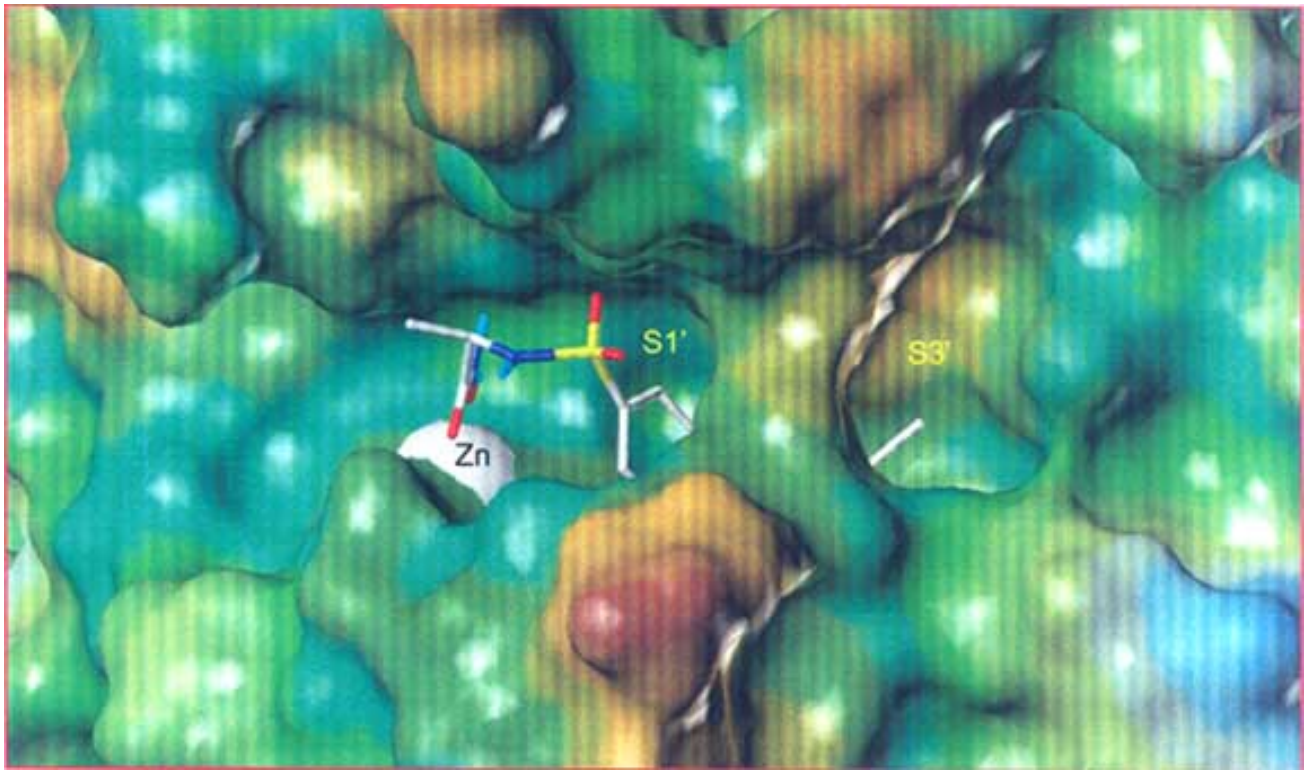

Fig. (13). X-ray structure of **9** bound to TACE. The protein is represented by its solvent accessible surface, and colored by lipophilic potential [brown = hydrophobic, blue = hydrophilic, green = neutral].

yield erroneous predictions. Nevertheless, the process of compensating for poor steric interactions by mobility is a delicate balancing act where other binding factors also play important roles. Clearly, just the presence of motion is not sufficient to compensate for the poor fit in the S1' pocket and yield a high-affinity binder, since other efforts have successfully capitalized on a poor fit to yield selective MMP inhibitors.

Compound 11 Complexed to TACE

The structure of pyrazolopyridine **11** [69] revealed another way of obtaining selectivity against the MMPs, through steric clashes and chemical differences afforded by non-conserved residues. In general, the binding mode of **11**, a 30 nM inhibitor of TACE, is very similar to that of **9** described above. The butynyl tail spans the S1'-S3' tunnel, the phenyl ring stacks against the active site histidine, a sulfonamide oxygen hydrogen bonds to the backbone NH's, and the hydroxamate chelates the zinc while also hydrogen bonding to nearby active site residues. The main differences in binding are attributed to the small positional changes of the atoms due to the extra carbon between the sulfonamide and hydroxamate moieties, and the introduction of the pyrazolopyridine ring system. Although these changes appear to move the atoms away from making ideal enthalpic interactions with the protein, the indazole-like ring system favorably contacts T347. In MMP-1, for example (IC50 ~1 μM), T347 is replaced by an asparagine residue, which cannot make the same interactions with the ring system. This residue is a leucine in both MMP-9 and MMP-13 (IC_{50}s of 116 nM and 80 nM, respectively).

CONCLUSION

The MMPs and TACE are very active and attractive targets for the design of therapeutic agents for a variety of diseases, in particular, cancer and arthritis. An abundance of NMR and X-ray structural information has been obtained for multiple members of the MMP family and TACE complexed to numerous inhibitors from diverse chemical classes. The availability of these structural data has been critical for the iterative design of the next generation of potent and selective inhibitors. The MMP structures have identified a clear mechanism to design inhibitors selective for a particular MMP by taking advantage of the unique size, shape and chemical features of its S1' pocket. A complicating factor in the design effort has been the observation of both MMP and inhibitor dynamics. The elasticity of the MMP active-site combined with inhibitor mobility enables compounds predicted to be poor binders based on static models to inhibit MMPs with high-affinity. However, with the accumulation of more structural-activity and NMR data, it is conceivable that chemists could use protein dynamics to their advantage. The desire to identify selective MMP inhibitors has been inferred from recent clinical trials where the common side effect of musculoskeletal problems may be attributed to broad inhibition of MMPs and/or other zinc containing enzymes.

ACKNOWLEDGEMENTS

The authors would like to thank Zhang-Bao Xu, James Chen, Eric Feyfant, Kevin Parris, Franklin J. Moy, Mary Geck and Weixin Xu for their contributions and suggestions in the preparation of this manuscript.

REFERENCES

[1] Ravanti, L.; Kahari, V.-M.; Matrix Metalloproteinases in Wound Repair. *Int. J. Mol. Med.* **2000**, *6*, 391-407.

[2] Vu, T. H.; Werb, Z.; Matrix Metalloproteinases: Effectors of Development and Normal Physiology. *Genes Dev.* **2000**, *14*, 2123-2133.

[3] Sternlicht, M. D.; Werb, Z.; How Matrix Metalloproteinases Regulate Cell Behavior. *Ann. Rev. Cell Dev. Biol.* **2001**, *17*, 463-516.

[4] McCawley, L. J.; Matrisian, L. M.; Matrix Metalloproteinases: They're Not Just for Matrix Anymore. *Curr. Opin. Cell Biol.* **2001**, *13*, 534-540.

[5] Skiles, J. W.; Gonnella, N. C.; Jeng, A. Y.; The Design, Structure, and Therapeutic Application of Matrix Metalloproteinase Inhibitors. *Curr. Med. Chem.* **2001**, *8*, 425-474.

[6] Nagase, H.; Woessner, J. F., Jr.; Matrix metalloproteinases. *J Biol Chem* **1999**, *274*, 21491-21494.

[7] Zask, A.; Levin, J. I.; Killar, L. M.; Skotnicki, J. S.; Inhibition of Matrix Metalloproteinases: Structure Based Design. *Curr. Pharm. Des.* **1996**, *2*, 624-661.

[8] Sternlicht, M. D.; Coussens, L. M.; Vu, T. H.; Werb, Z.; Biology and Regulation of the Matrix Metalloproteinases. *Matrix Metalloproteinase Inhibitors in Cancer Therapy*; Humana Press Inc., Totowa, N. J.: Department of Anatomy, UCSF, San Francisco, CA, USA, 2001; pp. 1-37.

[9] Ries, C.; Petrides, E.; Cytokine Regulation of Matrix Metalloproteinase Activity and its Regulatory Dysfunction in Disease. *Biol. Chem. Hoppe-Seyler* **1995**, *376*, 345-355.

[10] Woessner, J. F., Jr.; Matrix Metalloproteinases and Their Inhibitors in Connective Tissue Remodeling. *FASEB J.* **1991**, *5*, 2145-2154.

[11] Fingleton, B.; Matrisian, L. M.; Matrix Metalloproteinases in Cancer. *Matrix Metalloproteinase Inhibitors in Cancer Therapy*; Humana Press Inc., Totowa, N. J.: Department of Cell Biology, Vanderbilt University Medical Center, Nashville, TN, USA, 2001; pp 85-112.

[12] Shaw, T.; Inhibition of Matrix Metalloproteinases in Rheumatoid Arthritis. *Rheumatoid Arthritis*; Oxford University Press, Oxford, UK.: Roche Products Ltd, Welwyn Garden City, UK, 2000; pp. 551-561.

[13] Leppert, D.; Lindberg, R. L. P.; Kappos, L.; Leib, S. L.; Matrix Metalloproteinases: Multifunctional Effectors of Inflammation in Multiple Sclerosis and Bacterial Meningitis. *Brain Res. Rev.* **2001**, *36*, 249-257.

[14] Ulisse, S.; Della Riccia, D.; Cifone, M. G.; De Simone, C.; Matrix Metalloproteinases and Periodontopathies. *EOS--Riv. Immunol.* **2001**, *21*, 17-21.

[15] Miller, A.; Ben-Yosef, Y.; Braker, C.; Shapiro, S.; Matrix Metalloproteinases and Their Inhibitors in Hypoxia/Reoxygenation and Stroke. *Inflammation and Stroke*; Birkhaeuser Verlag, Basel, Switz: CS Neuroimmunlogy Research Units, Carmel Medical Center, Haifa, 34362, Israel, 2001; pp 275-285.

[16] Ciccocioppo, R.; Di Sabatino, A.; Corazza, G. R.; Matrix Metalloproteinases and the Gastrointestinal Tract. *EOS--Riv. Immunol.* **2001**, *21*, 9-13.

[17] Li, Y. Y.; Feldman, A. M.; Matrix Metalloproteinases in the Progression of Heart Failure: Potential Therapeutic Implications. *Drugs* **2001**, *61*, 1239-1252.

[18] Birkedal-Hansen, H.; Moore, W. G. I.; Bodden, M. K.; Windsor, L. J.; Birkedal-Hansen, B.; DeCarlo, A.; Engler, J. A.; Matrix Metalloproteinases: a Review. *Crit. Rev. Oral Biol. Med.* **1993**, *4*, 197-250.

[19] Rockwell, A.; Melden, M.; Copeland, R. A.; Hardman, K.; Decicco, C. P.; DeGrado, W. F.; Complementarity of Combinatorial Chemistry and Structure-Based Ligand Design: Application to the Discovery of Novel Inhibitors of Matrix Metalloproteinases. *J . Am . Chem . Soc* **1996**, *118*, 10337-10338.

[20] Hajduk, P. J.; Sheppard, G.; Nettesheim, D. G.; Olejniczak, E.; Discovery of Potent Nonpeptide Inhibitors of Stromelysin using SAR by NMR. *J. Am. Chem. Soc.* **1997**, *119*, 5818-5827.

[21] Olejniczak, E. T.; Hajduk, P. J.; Marcotte, P. A.; Nettesheim, D. G.; Stromelysin Inhibitors Designed from Weakly Bound Fragments: Effects of Linking and Cooperativity. *J. Am. Chem. Soc.* **1997**, *119*, 5828-5832.

[22] Ghose, A. K.; Logan, M. E.; Treasurywala, A. M.; Wang, H.; Wahl, R. C.; Tomczuk, B. E.; Gowravaram, M. R.; Jaeger, E. P.; Wendoloski, J. J.; Determination of Pharmacophoric Geometry for Collagenase Inhibitors Using a Novel Computational Method and Its Verification Using Molecular Dynamics, NMR and X-ray Crystallography. *J. Am. Chem. Soc* **1995**, *117*, 4671-4682.

[23] Lovejoy, B.; Welch, A. R.; Carr, S.; Luong, C.; Broka, C.; Hendricks, R. T.; Campbell, J. A.; Walker, K. A. M.; Martin, R.; Van Wart, H.; Browner, M. F.; Crystal Structures of MMP-1 and -13 Reveal the Structural Basis for Selectivity of Collagenase Inhibitors. *Nat. Struct. Biol.* **1999**, *6*, 217-221.

[24] Ishiguro, N.; Kojima, T.; Ito, T.; Iwata, H.; Matrix Metalloproteinase: Candidate for Clinical Joint Destruction Marker in Arthropathy. *Connect. Tissue* **2001**, *33*, 43-49.

[25] Vincenti, M. P.; Brinckerhoff, C. E.; The Potential of Signal Transduction Inhibitors for the Treatment of Arthritis: Is it all just JNK? *J. Clin. Invest.* **2001**, *108*, 181-183.

[26] Vincenti, M. P.; The Matrix Metalloproteinase (MMP) and Tissue Inhibitor of Metalloproteinase (TIMP) Genes: Transcriptional and Posttranscriptional Regulation, Signal Transduction and Cell-type-specific Expression. *Method. Molec. Biol.* **2001**, *151*, 121-148.

[27] Heath, E. I.; Grochow, L. B.; Clinical Potential of Matrix Metalloprotease Inhibitors in Cancer Therapy. *Drugs* **2000**, *59*, 1043-1055.

[28] Elliott, S.; Cawston, T.; The Clinical Potential of Matrix Metalloproteinase Inhibitors in the Rheumatic Disorders. *Drug. Aging* **2001**, *18*, 87-99.

[29] Holmbeck, K.; Bianco, P.; Caterina, J.; Yamada, S.; Kromer, M.; Kuznetsov, S. A.; Mankani, M.; Robey, P. G.; Poole, A. R.; Pidoux, I.; Ward, J. M.; Birkedal-Hansen, H.; MT1-MMP-Deficient Mice Develop Dwarfism, Osteopenia, Arthritis, and Connective Tissue Disease due to Inadequate Collagen Turnover. *Cell* **1999**, *99*, 81-92.

[30] Zhou, Z.; Apte, S. S.; Soininen, R.; Cao, R.; Baaklini, G. Y.; Rauser, R. W.; Wang, J.; Cao, Y.; Tryggvason, K.; Impaired Endochondral Ossification and Angiogenesis in Mice Deficient in Membrane-type Matrix Metalloproteinase I. *Proc. Nat. Acad. Sci. USA* **2000**, *97*, 4052-4057.

[31] Zhao, J.; Chen, H.; Peschon, J. J.; Shi, W.; Zhang, Y.; Frank, S. J.; Warburton, D.; Pulmonary Hypoplasia in Mice Lacking Tumor Necrosis Factor-alpha Converting Enzyme Indicates an Indispensable Role for Cell Surface Protein Shedding during Embryonic Lung Branching Morphogenesis. *Dev. Biol.* **2001**, *232*, 204-218.

[32] Baxter, A. D.; Bird, J. B.; Bannister, R.; Bhogal, R.; Manallack, D. T.; Watson, R. W.; Owen, D. A.; Montana, J.; Henshilwood, J.; Jackson, R.; C. D1927 and D2163: Novel Mercaptoamide Inhibitors of Matrix Metalloproteinases. *Cancer Drug Discovery and Development: Matrix Metalloproteinase Inhibitors in Cancer Therapy*; Humana Press, Inc.: Totowa, NJ, 2000; pp. 193-221.

[33] Shalinsky, D. R.; Shetty, B.; Pithavala, Y.; Bender, S.; Neri, A.; Webber, S.; Appelt, K.; Collier, M.; Prinomastat. A Potent and Selective Matrix Metalloproteinase Inhibitor—Preclinical and Clinical Development for Oncology. *Cancer Drug Discovery and Development: Matrix Metalloproteinase Inhibitors in Cancer Therapy*; Humana Press, Inc.: Totowa, NJ, 2000; pp. 143-173.

[34] Moy, F. J.; Pisano, M. R.; Chanda, P. K.; Urbano, C.; Killar, L. M.; Sung, M.-L.; Powers, R.; Assignments, Secondary Structure and Dynamics of the Inhibitor-free Catalytic Fragment of Human Fibroblast Collagenase. *J. Biomol. NMR* **1997**, *10*, 9-19.

[35] Moy, F. J.; Chanda, P. K.; Cosmi, S.; Pisano, M. R.; Urbano, C.; Wilhelm, J.; Powers, R.; High-Resolution Solution Structure of the Inhibitor-Free Catalytic Fragment of Human Fibroblast Collagenase Determined by Multidimensional NMR. *Biochemistry* **1998**, *37*, 1495-1504.

[36] Moy, F. J.; Chanda, P. K.; Chen, J. M.; Cosmi, S.; Edris, W.; Skotnicki, J. S.; Wilhelm, J.; Powers, R.; NMR Solution Structure of the Catalytic Fragment of Human Fibroblast Collagenase Complexed with a Sulfonamide Derivative of a Hydroxamic Acid Compound. *Biochemistry* **1999**, *38*, 7085-7096.

[37] Borkakoti, N.; Winkler, F. K.; Williams, D. H.; D'Arcy, A.; Broadhurst, M. J.; Brown, P. A.; Johnson, W. H.; Murray, E. J.; Structure of the Catalytic Domain of Human Fibroblast Collagenase Complexed with an Inhibitor. *Nat. Struct. Biol.* **1994**, *1*, 106-110.

[38] Lovejoy, B.; Cleasby, A.; Hassell, A. M.; Structural Analysis of the Catalytic Domain of Human Fibroblast Collagenase. *Ann. N.Y. Acad. Sci.* **1994**, *732*, 375-378.

[39] Lovejoy, B.; Cleasby, A.; Hassell, A. M.; Structure of the Catalytic Domain of Fibroblast Collagenase Complexed with an Inhibitor. *Science* **1994**, *263*, 375-377.

[40] Spurlino, J. C.; Smallwood, A. M.; Carlton, D. D.; Banks, T. M.; Vavra, K. J.; Johnson, J. S.; Cook, E. R.; Falvo, J.; Wahl, R. C.; Wendoloski, J. J.; Smith, D. L.; 1.56 A Structure of Mature Truncated Human Fibroblast collagenase. *Proteins: Struct., Funct., Genet.* **1994**, *19*, 98-109.

[41] Lovejoy, B.; Hassell, A. M.; Luther, M. A.; Crystal Structures of Recombinant 19-kDa Human Fibroblast Collagenase Complexed to Itself. *Biochemistry* **1994**, *33*, 8207-8217.

[42] Moy, F. J.; Chanda, P. K.; Cosmi, S.; Edris, W.; Levin, J. I.; Powers, R.; 1H, 15N, 13C, and 13CO Assignments and Secondary Structure Setermination of Collagenase-3 (MMP-13) Complexed with a Hydroxamic Acid Inhibitor. *J. Biomol. NMR* **2000**, *17*, 269-270.

[43] Moy, F. J.; Chanda, P. K.; Chen, J. M.; Cosmi, S.; Edris, W.; Levin, J. I.; Powers, R.; High-resolution Solution Structure of the Catalytic Fragment of Human Collagenase-3 (MMP-13) Complexed with a Hydroxamic Acid Inhibitor. *J. Mol. Biol.* **2000**, *302*, 671-689.

[44] Maskos, K.; Fernandez-Catalan, C.; Huber, R.; Bourenkov, G. P.; Bartunik, H.; Ellestad, G. A.; Reddy, P.; Wolfson, M. F.; Rauch, C. T.; Castner, B. J.; Davis, R.; Clarke, H. R. G.; Petersen, M.; Fitzner, J. N.; Cerretti, D. P.; March, C. J.; Paxton, R. J.; Black, R. A.; Bode, W.; Crystal Structure of the Catalytic Domain of Human Tumor Necrosis Factor-alpha Converting Enzyme. *Proc. Nat. Acad. Sci. USA* **1998**, *95*, 3408-3412.

[45] DiMartino, M.; Wolff, C.; High, W.; Stroup, G.; Hoffman, S.; Laydon, J.; Lee, J. C.; Bertolini, D.; Galloway, W. A.; Crimmin, M. J.; Davis, M.; Davies, S.; Anti-arthritic Activity of Hydroxamic Acid-based Pseudopeptide Inhibitors of Matrix Metalloproteinases and TNF-alpha Processing. *Inflamm. Res.* **1997**, *46*, 211-215.

[46] Powers, R.; Clore, G. M.; Garrett, D. S.; Gronenborn, A. M.; Relationships Between the Precision of High-Resolution Protein NMR Structures, Solution-order Parameters, and Crystallographic B Factors. *J. Magn. Reson., Ser. B* **1993**, *101*, 325-327.

[47] Sahu, S. C.; Bhuyan, A. K.; Majumdar, A.; Udgaonkar, J. B.; Backbone Dynamics of Barstar: a ^{15}N NMR Relaxation Study. *Proteins: Structure, Function, and Genetics* **2000**, *41*, 460-474.

[48] Pang, Y.; Buck, M.; Zuiderweg, E. R. P.; Backbone Dynamics of the Ribonuclease Binase Active Site Area Using Multinuclear (^{15}N and ^{13}CO) NMR Relaxation and Computational Molecular Dynamics. *Biochemistry* **2002**, *41*, 2655-2666.

[49] Uhrinova, S.; Smith, M. H.; Jameson, G. B.; Uhrin, D.; Sawyer, L.; Barlow, P. N.; Structural Changes Accompanying pH-Induced Dissociation of the β-Lactoglobulin Dimer. *Biochemistry* **2000**, *39*, 3565-3574.

[50] Zhang, P.; Dayie, K. T.; Wagner, G.; Unusual Lack of Internal Mobility and Fast Overall Tumbling in Oxidized Flavodoxin from Anacystis Nidulans. *J. Mol. Biol.* **1997**, *272*, 443-455.

[51] Constantine, K. L.; Friedrichs, M. S.; Goldfarb, V.; Jeffrey, P. D.; Sheriff, S.; Mueller, L.; Characterization of the Backbone Dynamics of an Anti-digoxin Antibody VL Domain by Inverse Detected Proton-Nitrogen-15 NMR: Comparisons with X-ray Data for the Fab. *Proteins: Struct., Funct., Genet.* **1993**, *15*, 290-311.

[52] Yuan, P.; Marshall, V. P.; Petzold, G. L.; Poorman, R. A.; Stockman, B. J.; Dynamics of Stromelysin/Inhibitor Interactions Studied by 15N NMR Relaxation Measurements: Comparison of Ligand Binding to the S1-S3 and S1'-S3' Subsites. *J. Biomol. NMR* **1999**, *15*, 55-64.

[53] Zhang, X.; Gonnella, N. C.; Koehn, J.; Pathak, N.; Ganu, V.; Melton, R.; Parker, D.; Hu, S.-I.; Nam, K.-Y.; Solution structure of the catalytic domain of human collagenase-3 (MMP-13) complexed to a potent non-peptidic sulfonamide inhibitor: Binding comparison with stromelysin-1 and collagenase-1. *J. Mol. Biol.* **2000**, *301*, 513-524.

[54] Moy, F. J.; Chanda, P. K.; Chen, J., M.; Cosmi, S.; Edris, W.; Levin, J., I.; Wilhelm, J.; Rush, T. S.; Powers, R.; Impact of Mobility on Structure-Based Drug Design for the MMPs. *J. Am. Chem. Soc.* **2002**, *124*, 12658-12659.

[55] Ferentz, A. E.; Wagner, G.; NMR Spectroscopy: a Multifaceted Approach to Macromolecular Structure. *Q. Rev. Biophys.* **2000**, *33*, 29-65.

[56] Roberts, G. C. K.; Applications of NMR in Drug Discovery. *Drug Discov. Today* **2000**, *5*, 230-240.

[57] Gubernator, K.; Boehm, H. J.; Examples of Active Areas of Structure Based Design. *Methods Princ. Med. Chem* **1998**, *6*, 15-36.

[58] Kubinyi, H.; Structure-Based Design of Enzyme Inhibitors and Receptor Ligands. *Curr. Opin. Drug Discovery Dev.* **1998**, *1*, 4-15.

[59] Gane, P. J.; Dean, P. M.; Recent Advances in Structure-Based Rational Drug Design. *Curr. Opin. Struct. Biol.* **2000**, *10*, 401-404.

[60] Joseph-McCarthy, D.; Computational Approaches to Structure-Based Ligand Design. *Pharmacol. Ther.* **1999**, *84*, 179-191.

[61] Gonnella, N. C.; Li, Y.-C.; Zhang, X.; Paris, C. G.; Bioactive Conformation of a Potent Stromelysin Inhibitor Determined by X-Nucleus Filtered and Multidimensional NMR Spectroscopy. *Bioorg. Med. Chem.* **1997**, *5*, 2193-2201.

[62] Li, Y.-C.; Zhang, X.; Melton, R.; Ganu, V.; Gonnella, N. C.; Solution Structure of the Catalytic Domain of Human Stromelysin-1 Complexed to a Potent, Nonpeptidic Inhibitor. *Biochemistry* **1998**, *37*, 14048-14056.

[63] Levin, J. I.; Du, M. T.; DiJoseph, J. F.; Killar, L. M.; Sung, A.; Walter, T.; Sharr, M. A.; Roth, C. E.; Moy, F. J.; Powers, R.; Jin, G.; Cowling, R.; Skotnicki, J. S.; The Discovery of Anthranilic Acid-based MMP Inhibitors. 1. SAR of the 3-position. *Bioorg. Med. Chem. Lett.* **2001**, *11*, 235-238.

[64] Chen, J. M.; Nelson, F. C.; Levin, J. I.; Mobilio, D.; Moy, F. J.; Nilakantan, R.; Zask, A.; Powers, R.; Structure-Based Design of a Novel, Potent, and Selective Inhibitor for MMP-13 Utilizing NMR Spectroscopy and Computer-Aided Molecular Design. *J. Am. Chem. Soc.* **2000**, *122*, 9648-9654.

[65] Levin, J. I.; Chen, J.; Du, M.; Hogan, M.; Kincaid, S.; Nelson, F. C.; Venkatesan, A. M.; Wehr, T.; Zask, A.; DiJoseph, J.; Killar, L. M.; Skala, S.; Sung, A.; Sharr, M.; Roth, C.; Jin, G.; Cowling, R.; Mohler, K. M.; Black, R. A.; March, C. J.; Skotnicki, J. S.; The Discovery of Anthranilic Acid-based MMP Inhibitors. 2. SAR of the 5-position and P1' Groups. *Bioorg. Med. Chem. Lett.* **2001**, *11*, 2189-2192.

[66] Aranapakam, V.; Davis, J. M.; Grosu, G. T.; Baker, J.; Ellingboe, J.; Zask, A.; Levin, J. I.; Sandanayaka, V. P.; Du, M.; Skotnicki, J. S.; DiJoseph, J. F.; Sung, A.; Sharr, M. A.; Killar, L. M.; Walter, T.; Jin, G.; Cowling, R.; Tillett, J.; Zhao, W.; McDevitt, J.; Xu, Z.-B.; Synthesis and Structure-activity Relationship of N-Substituted 4-arylsulfonylpiperidine-4-hydroxamic acids as Novel Orally Active Matrix Metalloproteinase Inhibitors for the Treatment of Osteoarthritis. *J. Med. Chem.* **2003**, In press.

[67] Chen, J. M.; Jin, G.; Sung, A.; Levin, J. I.; Anthranilate sulfonamide hydroxamate TACE inhibitors. Part 1: Structure-based design of novel acetylenic P1' groups. *Bioorg. Med. Chem. Lett.* **2002**, *12*, 1195-1198.

[68] Levin, J. I.; Chen, J. M.; Du, M. T.; Nelson, F. C.; Killar, L. M.; Skala, S.; Sung, A.; Jin, G.; Cowling, R.; Barone, D.; March, C. J.; Mohler, K. M.; Black, R. A.; Skotnicki, J. S.; Anthranilate sulfonamide hydroxamate TACE inhibitors. Part 2: SAR of the acetylenic P1' group. *Bioorg. Med. Chem. Lett.* **2002**, *12*, 1199-1202.

[69] Zask, A.; Gu, Y.; Albright, J. D.; Du, X.; Hogan, M.; Levin, J. I.; Chen, J. M.; Killar, L. M.; Sung, A.; DiJoseph, J. F.; Sharr, M. A.; Roth, C. E.; Skala, S.; Jin, G.; Cowling, R.; Mohler, K. M.; Barone, D.; Black, R.; March, C.; Skotnicki, J. S.; Synthesis and SAR of bicyclic heteroaryl hydroxamic acid MMP and TACE inhibitors. *Bioorg. Med. Chem. Lett.* **2003**, *13*, 1487-1490.

[70] Levin, J. I.; Chen, J. M.; Cheung, K.; Cole, D.; Crago, C.; Santos, E. D.; Du, X.; Khafizova, G.; MacEwan, G.; Niu, C.; Salaski, E. J.; Zask, A.; Cummons, T.; Sung, A.; Xu, J.; Zhang, Y.; Xu, W.; Ayral-Kaloustian, S.; Jin, G.; Cowling, R.; Barone, D.; Mohler, K. M.; Black, R. A.; Skotnicki, J. S.; Acetylenic TACE inhibitors. Part 1. SAR of the acyclic sulfonamide hydroxamates. *Bioorg. Med. Chem. Lett.* **2003**, *13*, 2799-2803.